JOURNAL OF AIRCRAFT
Vol. 33, No. 3, May–June 1996

Evaluation of Transition in Flight Tests Using Nonlinear Parabolized Stability Equation Analysis

Géza Schrauf*
Daimler–Benz AG, 28183 Bremen, Germany
and
Thorwald Herbert† and Greg Stuckert‡
DynaFlow, Inc., Columbus, Ohio 43221

The VFW 614/ATTAS flight tests have provided an extensive database for the analysis and development of methods to predict transition for aerodynamic design. While previous work has rested on the e^N method, we re-evaluate two Tollmien–Schlichting-dominated test cases using the linear and nonlinear parabolized stability equations (PSE). We compare results obtained by standard, linear local stability theory with results obtained by linear PSE, investigate possible transition mechanisms for the two test cases, and perform parametric studies to estimate the initial amplitudes to start the PSE calculations.

Introduction

THE tools currently used to design laminar wings are based on the e^N method.[1,2] Ideally, the design engineer would like to have one or two universal values of the N factor to decide on the transition location. Numerous strategies have been developed to produce such values by integrating the amplification rates provided by the linear stability theory in more or less physical ways.[3–5] While success has been reported for some efforts,[6] the value of the e^N method has been questioned by others.[7] Obviously, the linear theory of primary instabilities cannot explain the complex nonlinear transition phenomena and their dependence on the disturbance level. However, in the absence of a practical nonlinear approach, the e^N method has been more successful than previous criteria based on lump parameter values that completely ignore the stability characteristics of the flow.

A variety of N factor integration strategies were applied by Schrauf[8] to evaluate the flight tests with the VFW 614/ATTAS aircraft. These flight tests covered a range from Tollmien–Schlichting (TS)- to crossflow (CF)-dominated conditions. No universal N factor could be found with the envelope method. Strategies that adhere to physical constraints provide more consistent values, though they are different for TS- and CF-dominated cases. Ironically, use of the incompressible stability theory gives more consistent results in the Mach number range $0.3 \leq M_\infty \leq 0.7$ of the flight tests.

A new approach to transition analysis based on parabolized stability equations (PSE) was proposed by Herbert.[9] The PSE form an initial-boundary-value problem that can be solved with efficient marching techniques, more efficient than direct numerical simulation (DNS) for the Navier–Stokes equations. The linear problem, as well as the nonlinear problems of secondary instability and mode interactions can be treated. Nonlinear studies on instabilities and transition in the flat-plate boundary layer[10,11] have shown good agreement with DNS results and experiments. A discussion of the linear and nonlinear PSE and their applications have been given by Herbert.[12]

If the atmospheric and surface conditions as well as the related receptivity mechanisms were known, the nonlinear PSE method could predict transition from first principles. Lacking this information, we will exploit the current body of knowledge and apply the nonlinear PSE to re-evaluate some of the VFW 614/ATTAS flight tests.

ATTAS Flight Tests

Sponsored by the German laminar-flow research program, the VFW 614 aircraft of the DLR was equipped with a laminar-flow glove (Fig. 1). The glove was designed to show the effects of TS and CF instability separately within the test envelope. The tests, carried out together with the DLR, covered Mach numbers from 0.35 to 0.7 and Reynolds numbers from 12×10^6 to 30×10^6. By flying with sideslip, the sweep angle could be varied from 18 to 24 deg. Pressure distributions were measured as input for the boundary-layer calculations and subsequent stability analysis. The transition location was detected by an IR image technique.

Two test cases were chosen for this investigation. Mach number, Reynolds number, geometrical as well as effective sweep angles, and the transition location are listed in Table 1.

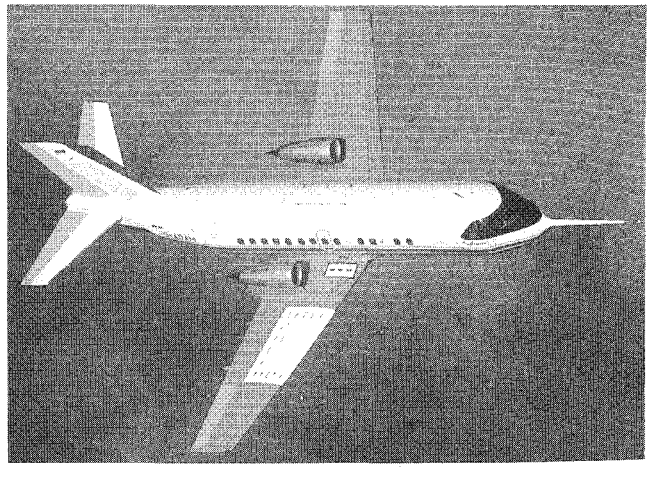

Fig. 1 VFW 614/ATTAS aircraft with laminar-flow glove.

Presented as Paper 95-1801 at the AIAA 13th Applied Aerodynamics Conference, San Diego, CA, June 19–22, 1995; received June 22, 1995; revision received Dec. 18, 1995; accepted for publication Jan. 8, 1996.

*Research Scientist. Member AIAA.
†Professor of Mechanical Engineering, P.O. Box 21319. Associate Fellow AIAA.
‡Research Scientist, P.O. Box 21319. Member AIAA.

Table 1 Flow conditions

Parameter	A	B
M	0.60	0.35
Re	15,700,000	12,200,000
φ_{GEO}	17.3 deg	17.6 deg
φ_{EFF}	21.9 deg	21.2 deg
Transition	40%	17%

Both cases are dominated by strong TS amplification. Case A exhibits moderate and case B weak growth of crossflow vortices. Crossflow-dominated cases will be considered later.[13]

Linear Analysis

The boundary layers were calculated with a modified version of the Kaups–Cebeci code[14] and the LISW code,[15] developed at Daimler–Benz AG, and stored in a database. This database was already used in the previous analysis[8] with the linear stability code COAST.[16] The boundary-layer files contain sufficient data for the traditional linear stability analysis (LST), but not for PSE analysis, which also requires the streamwise derivatives of the velocity components and the small velocity component normal to the wing surface. To avoid discrepancies caused by different boundary-layer profiles, the data of the boundary-layer database are used here. Thus, for the analysis presented in this article, we neglect the normal velocity component as well as the streamwise derivatives of the boundary-layer flow. We also neglect curvature effects.

As a first task, the results of the two LST codes COAST and LISA (Ref. 17) for LST characteristics were validated. Similar comparisons between the results of COAST and the codes used at CERT/ONERA were performed for an infinitely long, swept cylinder[18] and for the F100 flight experiments within the European ELFIN I/II programs.[19] Already with moderate resolution, e.g., 50 points in normal direction, the amplification rates for TS waves and steady crossflow vortices agree within a relative error of 1% between COAST and LISA. The eigenfunctions are often indistinguishable within plotting accuracy as shown in Fig. 2.

To present comparisons between LST and linear PSE analysis, we chose test case A with strong TS and moderate CF amplification. The N-factor evolution of the TS and stationary CF wave with the largest N factors at transition is plotted in Fig. 3. Comparisons of the local spatial amplification rates obtained with the LST codes COAST and LISA as well as with the PSE code COPS (Ref. 20) are shown in Figs. 4 and 5. We observe that for the TS wave the amplification rates obtained with LST and linear PSE are practically identical, whereas they are different for the crossflow vortex. This shows a posteriori

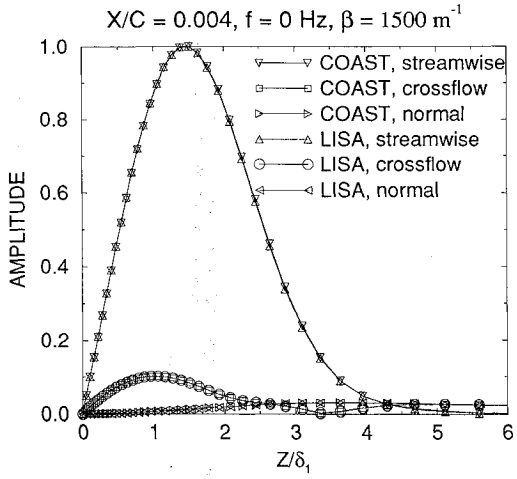

Fig. 2 Case A: velocity components of a crossflow eigenfunction computed with COAST and LISA.

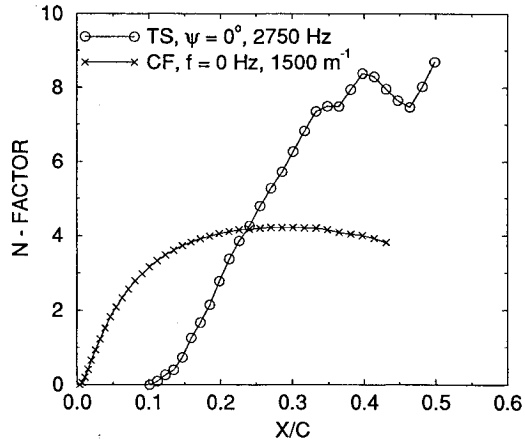

Fig. 3 Case A: TS and stationary CF wave with largest N factors at transition.

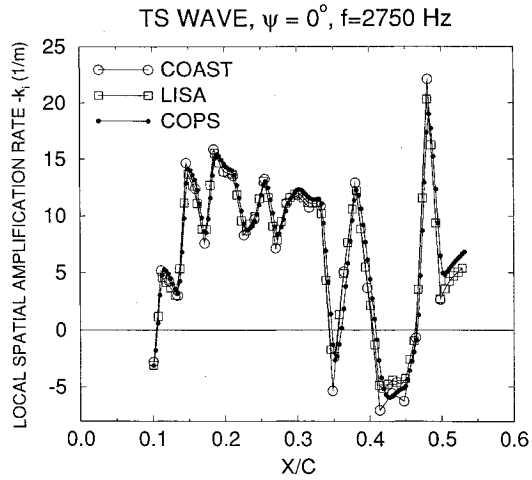

Fig. 4 Case A: dimensional local spatial amplification rates for the TS wave.

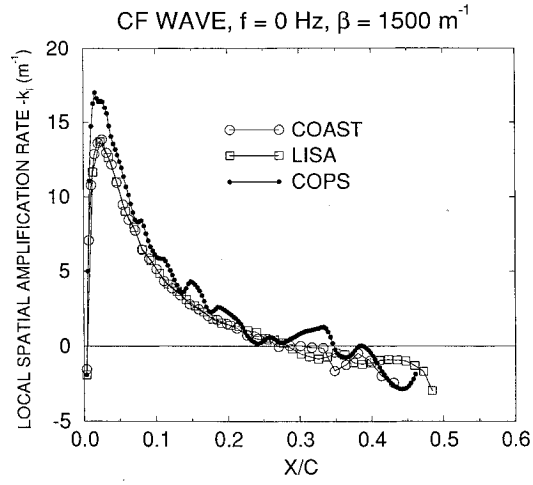

Fig. 5 Case A: dimensional local spatial amplification rates for the stationary CF wave.

that the TS-amplification rate does not depend on nonlocal effects.

We can calculate N factors from PSE results by taking the natural logarithm of the amplitude ratio A/A_0, where A is the current amplitude and A_0 is the amplitude at the neutral point. Again, PSE N factors are larger than LST N factors for crossflow waves (Fig. 6) and nearly identical for TS waves (Fig. 7).

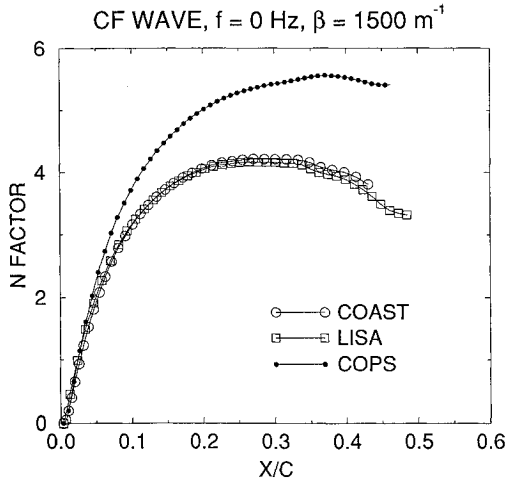

Fig. 6 Case A: *N* factors of the CF wave.

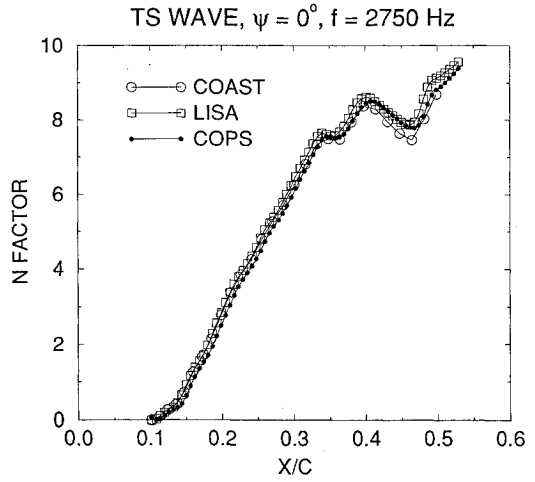

Fig. 7 Case A: *N* factors for the TS wave.

The importance of nonlocal effects for stationary crossflow vortices is heuristically obvious since a section of a stationary CF vortex feels the presence and the strength of the section upstream, i.e., the vortex pieces are not independent of each other. If they were, they would not align and create the streak pattern observed in transition visualization. TS waves behave differently: each wave propagates downstream independent of the waves upstream.

Nonlinear Analysis

Initial Amplitudes

The stability equations for the traditional, linear local theory are ordinary differential equations that form an eigenvalue problem. Only the shape of the eigenfunction is determined by the problem, because we can multiply the eigenfunction with any complex factor. For Fig. 2, we chose the factor such that the maximum of the streamwise velocity component becomes real and has the value of 1.

The parabolic stability equations constitute an initial-boundary-value problem. Besides boundary conditions, we also need initial conditions to start the calculation. In the previous section, we started the computations upstream of the neutral point and used the eigenfunction obtained by LST to determine the shape of the initial function. But with which value of the amplitude should we start the calculation? The best answer would require an understanding of the process by which external disturbances like freestream turbulence or surface roughness create Tollmien–Schlichting or crossflow waves in the boundary layer. Although significant progress concerning receptivity has been made, we are not yet able to calculate initial amplitudes because there is insufficient documentation of the environmental disturbances in free flight.

To make PSE calculations feasible for the design engineer, we need standard initial conditions. Lacking any information, we assume that disturbances in the oncoming freestream induce wave-like disturbances with a broad frequency range everywhere in the boundary layer. The disturbances induced upstream of the neutral point are damped out. The ones in the neighborhood of the neutral point play the most important role because they are maximally amplified. If the disturbances are induced further downstream, they are not so much amplified, and therefore, less noticeable.

With this in mind, we claim as a working hypothesis that there is a standard initial amplitude for TS waves, independent of the frequency and independent of the location of the neutral point.

For a first estimation of this amplitude, we note that, for TS-dominated transition, the amplitudes reach values of 10–15% at transition and that the N factor is between 9–11. From this, we obtain initial amplitudes of the order of 10^{-6} to 2×10^{-5} for Tollmien–Schlichting waves at the neutral point.

A similar argument holds for stationary crossflow vortices. We assume that these vortices are triggered by surface roughness or small-scale surface waviness that is equally distributed over the glove surface, i.e., we assume a uniform surface quality. Therefore, we may assume that the initial amplitude is independent of the position of the neutral point. We also assume that, at least for the strongly amplified crossflow vortices, the initial amplitude is independent of the wavelength, and of the dimensional spanwise wave number of the crossflow vortex.

Müller[21] and Saric[22] report that the amplitudes of the stationary crossflow waves reach 10–12% in the transition region. With an N factor of about 10 at transition, we arrive at initial amplitudes of the order of 5×10^{-6} for the crossflow vortices.

With these two hypotheses we can proceed to study the different interaction mechanisms.

TS/CF Interaction

One possible mechanism leading to the breakdown of laminarity is the interaction of a Tollmien–Schlichting wave with a weak crossflow vortex. To study this mechanism, we chose flight measurement B with strong TS and weak CF amplification. For this case, transition was observed at 17%. According to linear local theory, the TS wave with a frequency of 4000 Hz and the CF vortex with a spanwise wave number of 2000 m^{-1} are dominant at transition. The crossflow vortex has an N factor of 0.8 at the neutral point of the TS wave. Its N factor reaches only the value of 1 and decreases downstream of $X/C = 0.08$ until it becomes 0.6 in the transition region (cf., Fig. 8). Thus, according to the e^N method, the vortex with $\beta = 2000\ m^{-1}$ should have no influence on transition.

The nonlinear calculations are started just upstream of the neutral point of the TS wave at $X/C = 0.03$. For the first series we choose a fixed initial amplitude of $A_{CF,1} = 10^{-5}$ for the crossflow vortex, which corresponds to an initial amplitude of $A_{CF,0} = 5 \times 10^{-6}$ at its neutral point at $X/C = 0.004$. The initial amplitude of the TS wave is varied. For very small values the natural logarithm of the TS amplitude is identical to the shifted N-factor curve of Fig. 8. If the initial amplitude is increased to 2×10^{-7} (see Fig. 9), two oblique waves (these two modes are not symmetric because the boundary layer is not two dimensional), with the frequency of 4000 Hz and spanwise wave numbers of $\pm 2000\ m^{-1}$, are created by the nonlinear interaction of the TS wave with the crossflow vortex. Their growth is governed by the growth of the TS wave, because the CF amplification is weak. When the TS wave reaches a threshold amplitude of 0.8%, the two oblique waves interact with the already decaying crossflow vortex. Because the TS wave driv-

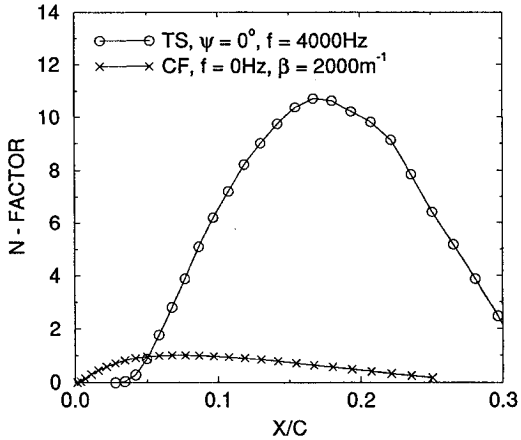

Fig. 8 Case B: TS and stationary CF wave with largest N factors at transition.

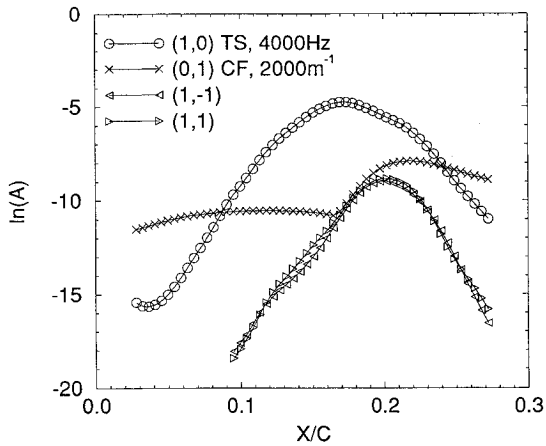

Fig. 9 Case B: TS/CF interaction with initial TS amplitude of 2×10^{-7}.

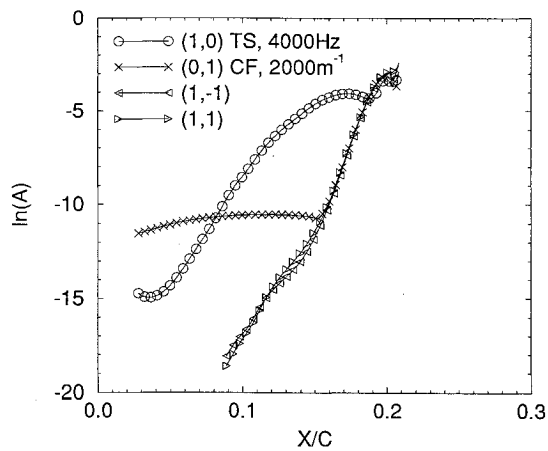

Fig. 10 Case B: TS/CF interaction with initial TS amplitude doubled to 4×10^{-7}.

ing the mechanism decays after reaching the threshold amplitude, there is no additional forcing and all waves decay.

Therefore, we doubled the initial TS amplitude to 4×10^{-7}, so that the TS wave reaches its critical amplitude of this time 1.1% somewhat earlier (Fig. 10). Again we observe the interaction of the two oblique modes with the decaying crossflow vortex. This time, however, the TS wave still grows sufficiently strong for the amplitudes of the three locked modes to reach the level of the TS amplitude, and all four waves interact. This results in additional growth, though without interaction each wave would decay. An estimated two TS wavelengths (about 1% chord) downstream of the interaction of all four modes, we expect the flow to become turbulent. This, of course, cannot be simulated by considering only four waves. In the following calculations we increased the TS amplitude to larger values. The qualitative behavior remains the same. Only the location X_3/C of the interaction of the two oblique modes with the crossflow vortex and the location X_4/C of the interaction of all four considered modes are shifted upstream. For an initial TS amplitude of 10^{-6}, X_4/C is 0.165, i.e., just upstream of the measured transition location (cf., Fig. 11).

In Fig. 12, the initial TS amplitudes are plotted over the location X_4/C. The best correlation of X_4/C with the transition location is obtained with an initial amplitude of 10^{-6}, consistent with the estimation of the previous section.

In our second series of calculations we varied the initial amplitude of the crossflow vortex. Again we find the interaction of the two oblique modes with the crossflow vortex when the TS amplitude reaches a threshold value of 1.5%. The coupled modes exhibit a strong growth. All four modes interact when their amplitudes reach the level of the TS amplitude. The positions X_3/C and X_4/C, however, are nearly independent of the choice of the initial CF amplitude, even if we reduce it, compared to the result shown in Fig. 11, by a factor of 10 and a factor of 1000 (cf., Fig. 13). The strong TS wave governs the scenario, and we are unable to estimate the initial CF amplitude using a parameter variation.

In the next calculation (Fig. 14), we show that the four modes, considered to this point, are in fact, the principal modes. We do this by repeating the calculation, including all modes with frequencies $n \times 4000$ Hz, $n = 0, 1, 2$ and spanwise wave numbers of $l \times 2000$ m^{-1}, $j = 0, \pm 1, \pm 2$, except the

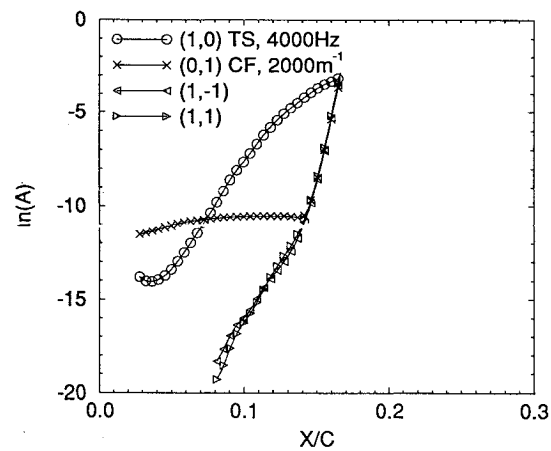

Fig. 11 Case B: TS/CF interaction with initial TS amplitude increased to 10^{-6}.

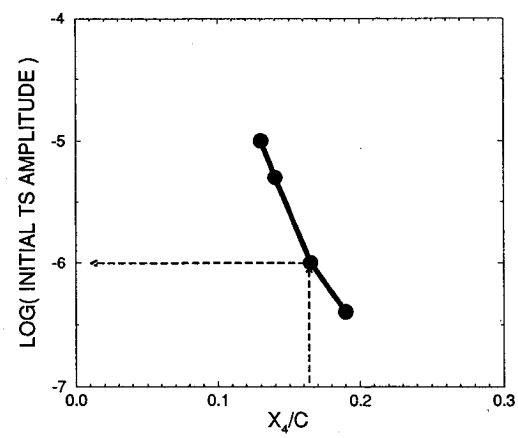

Fig. 12 Correlation of the location X_4/C with the observed transition location.

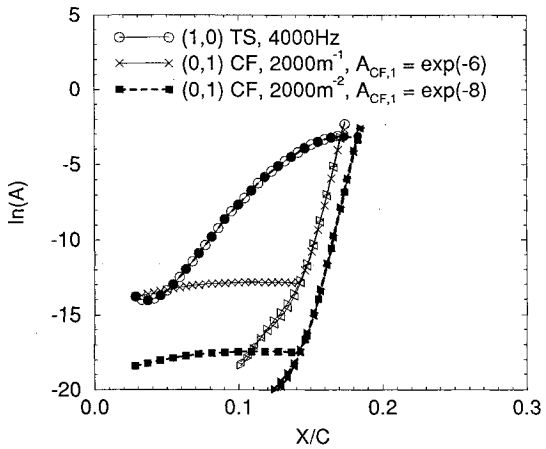

Fig. 13 Case B: two nonlinear PSE results with initial CF amplitudes of 10^{-6} and 10^{-8}.

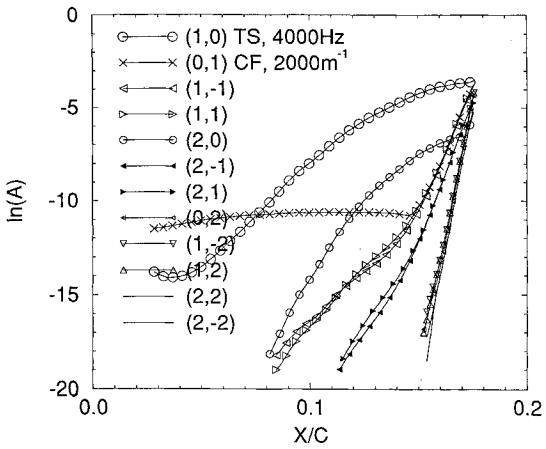

Fig. 14 Case B: recalculation of Fig. 11 allowing for 12 interacting modes.

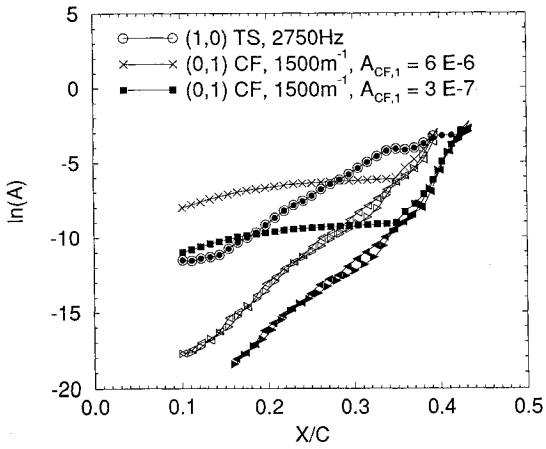

Fig. 15 Case A: TS/CF interaction for case A. Variation of the initial CF amplitude.

mode (0, 0). We see that the additional modes, though they are also growing strongly, are governed by the four principal modes and do not change the scenario.

Two results for the other flight measurement are shown in Fig. 15. As before, the TS wave dominates the interaction process. With a parameter variation, we obtain the best correlation of the transition location of the position X_4/C for TS amplitudes in the range of $1-5 \times 10^{-6}$. The CF initial amplitude is again less important, as can be seen from the relatively small shift of X_4/C from 0.395 to 0.415, even though the CF amplitude is reduced by a factor of 20. This case is, however, less suitable for a correlation, because small wiggles in the C_p distribution create wiggles in the TS amplitudes that cause small jumps in the location X_4/C.

Subharmonic Resonance

As a second model of TS-dominated transition, we analyze the subharmonic secondary instability.[23] In a three-dimensional boundary layer, this secondary instability (the subharmonic resonance) is different from its well-documented two-dimensional counterpart, because the crossflow velocity destroys the symmetry between the two oblique waves.

The typical development of the interaction proceeds in four phases that we present using flight measurement B. As before, we consider the Tollmien–Schlichting wave with frequency 2750 Hz, because it is the one with the largest N factor at transition. In addition to the TS wave, we choose two subharmonic oblique waves with $f = 1375$ Hz, $\beta = \mp 162$ m^{-1}, and a wave angle of $\Psi = \mp 52$ deg. Both waves are damped at the neutral point of the Tollmien–Schlichting wave.

We start our first run, using initial amplitudes of 10^{-6} for all three waves (cf., Fig. 16). As long as the amplitudes are small, all three waves travel independent of each other. Their propagation can be described by linear local theory. When the amplitude of the TS wave increases, the weaker of the two oblique waves is at some point forced to adjust its phase and to grow stronger until the amplitudes of both oblique waves have the same size. This occurs when the TS amplitude reaches a value of 0.25–0.5%, and concludes the second phase. In the third phase, both modes interlock and exhibit strong growth. When their amplitudes reach a level of about 2.5–3% (we found in some calculations values from 1.3 to 4%, i.e., this level is less sharp), the oblique waves interact with the TS wave and all three modes grow rapidly. Before that interaction, the growth of the TS wave can be described by local linear theory. Afterwards, the point of no-return is passed and the flow loses laminarity.

The beginning of phase three, i.e., the locking position of the two subharmonic waves, depends on the amplitude of the TS wave. It does not depend on the initial amplitudes of the two subharmonics. This can be seen in Fig. 17, where we increased the initial amplitudes of the subharmonics so much that their amplitudes do not fall below a level of 10^{-6}. We see that the locking of the two subharmonics happens at the same position, but, at a different amplitude level. Because the growth rate of the two locked modes is the same as before, the threshold level of 2.5% is reached earlier, resulting in an earlier rapid growth of all three waves.

We justify choosing the initial amplitudes such that the wave amplitudes do not fall below a certain minimal level by our assumption that disturbances in the oncoming flow create waves with a wide frequency and wave number range everywhere in the boundary layer.

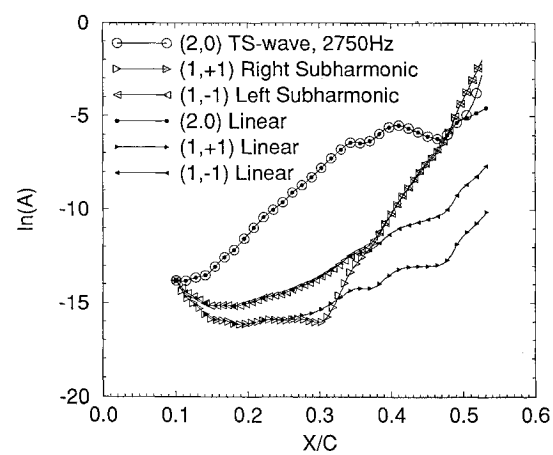

Fig. 16 Case A: subharmonic resonance. The linear development is included for comparison.

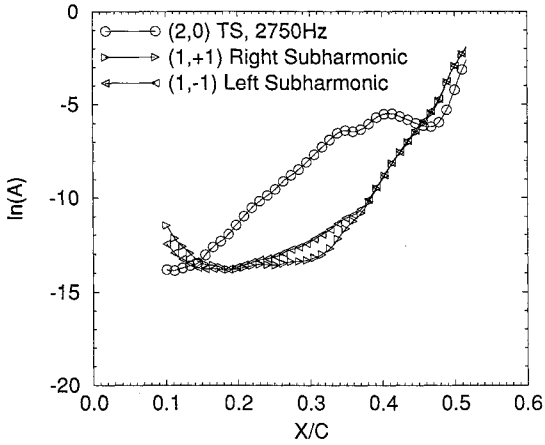

Fig. 17 Case A: subharmonic resonance with different initial amplitudes for the subharmonics.

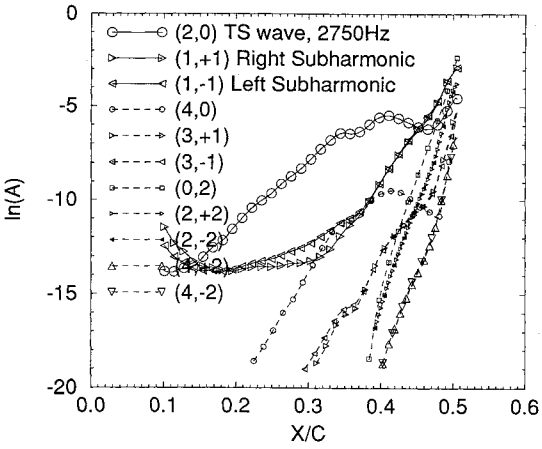

Fig. 18 Case A: subharmonic resonance with eight additional modes.

As before, a calculation with only three modes is far from being sufficient to further describe the breakdown to turbulence. In Fig. 18 we present a calculation with eight additional modes. It shows that those modes come into play relatively late and do not change the four-phase scenario.

In the results presented to this point, phase four starts downstream of the observed transition location of 40%. Because of this, we performed a parameter study by increasing the initial TS amplitude. For a value of 10^{-6} we found a good correlation with the experimentally observed transition location. In a second parameter variation using a TS wave with frequency 3200 Hz, we obtained the level of $3-4 \times 10^{-6}$ for the initial TS amplitude. This is the same range we previously got for the TS/CF interaction. Thus, at the moment we cannot decide which of the two possible mechanisms is more likely to be causing transition.

Combination Resonance

A third possibility for TS-dominated transition is the combination resonance. Instead of two oblique waves with half the frequency of the Tollmien–Schlichting wave, we consider two oblique waves with frequency $f_1 = \tau \cdot f_{TS}$ and $f_2 = (1 - \tau) \cdot f_{TS}$, such that their superposition gives the TS frequency. An example is given in Fig. 19. For combination resonance, the scenario is very similar to the one we encounter for subharmonic resonance. In this case, however, we have one more degree of freedom, namely, the value of τ. We found that the most sensitive cases are close to subharmonic resonance, that is, we obtain for a given TS initial amplitude the largest interaction for τ values between 0.5–0.25. The results are similar to those for subharmonic resonance: if the TS amplitude reaches a

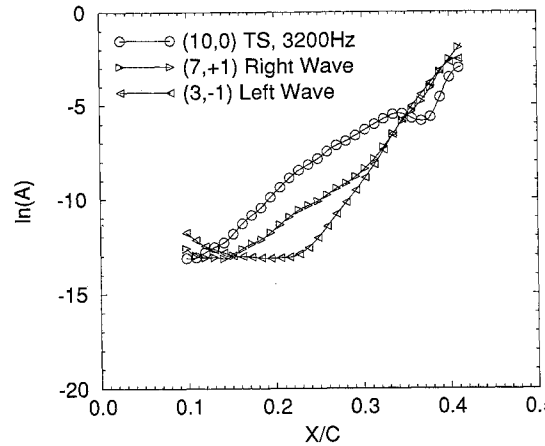

Fig. 19 Case B: combination resonance. $\beta = 232$ m^{-1}.

threshold value of 0.25–0.5%, both oblique modes interlock. The locked modes continue to grow. If their amplitudes reach a level of 3–4%, they interact with the TS wave and all three modes exhibit strong growth. This constitutes the point of no return and the laminarity of the flow breaks down.

Conclusions

Two flight tests with the VFW 614/ATTAS laminar flow glove have been analyzed. A comparison of the results obtained with standard, linear local stability theory and linear PSE showed that the amplification rates of crossflow vortices become larger if nonlocal effects are considered, whereas the amplification rates of Tollmien–Schlichting waves stay unchanged. Nonlinear PSE calculation show that there are three scenarios that could cause the laminar/turbulent transition, namely, TS/CF interaction, subharmonic resonance, and combination resonance.

To further develop nonlinear PSE calculations as tools for transition prediction, it is important to find standard initial amplitudes for each experiment. For the ATTAS flight test, we found a value of 10^{-6} for the initial amplitude of Tollmien–Schlichting waves.

Acknowledgments

This work is supported by Daimler–Benz AG in preparation of the national technology program Reduktion aerodynamischer Widerstand RaWiD (Cruise Drag Reduction), the Air Force Office of Scientific Research under Contract F49620-92-J-0271 (TH), and by the NASA Ames Research Center under Contract NAS2-13916 (TH & GKS).

References

[1]Van Ingen, J. L., "A Suggested Semi-Empirical Method for the Calculation of the Boundary Layer Transition Region," Univ. of Technology, Dept. of Aerospace Engineering, Rept. UTH-74, Delft, The Netherlands, 1956.

[2]Smith, A. M. O., and Gamberoni, A. H., "Transition, Pressure Gradient and Stability Theory," Douglas Aircraft Co., Rept. ES26388, El Segundo, CA, 1956.

[3]Schrauf, G., Bieler, H., and Thiede, P., "Transition Prediction—The Deutsche Airbus View," *Proceedings of the 1st European Forum on Laminar Flow Technology*, DGLR Rept. 92-06, 1992, pp. 73–82.

[4]Schrauf, G., "Curvature Effects for Three-Dimensional Compressible Boundary Layer Stability," *Zeitschrift für Flugwissenschaften und Weltraumforschung*, Vol. 16, No. 2, 1992, pp. 119–127.

[5]Arnal, D., "Boundary Layer Transition: Predictions Based on Linear Theory," *Special Course on Progress in Transition Modelling*, AGARD Rept. 793, pp. 2/1–63, 1994.

[6]Malik, M. R., "Stability for Laminar Flow Control Design," *Viscous Drag Reduction in Boundary Layers*, Progress in Astronautics and Aeronautics, AIAA, Washington, DC, Vol. 123, 1990, pp. 3–46.

[7]Morkovin, M. V., and Reshotko, E., "Dialogue on Progress and Issues in Stability and Transition Research," edited by D. Arnal and R. Michel, *Laminar-Turbulent Transition*, Springer–Verlag, Berlin, 1990.

[8]Schrauf, G., "Transition Prediction Using Different Linear Stability Analysis Strategies," AIAA Paper 94-1848, June 1994.

[9]Herbert, T., "Boundary-Layer Transition—Analysis and Prediction Revisited," AIAA Paper 91-0737, Jan. 1991.

[10]Bertolotti, F. P., Herbert, T., and Spalart, P. R., "Linear and Nonlinear Stability of the Blasius Boundary Layer," *Journal of Fluid Mechanics*, Vol. 242, 1992, pp. 441–474.

[11]Bertolotti, F. P., "Linear and Nonlinear Stability of Boundary Layers with Streamwise Varying Properties," Ph.D. Dissertation, Ohio State Univ., Columbus, OH, 1991.

[12]Herbert, T., "Parabolized Stability Equations," *Special Course on Progress in Transition Modelling*, AGARD Rept. 793, pp. 4/1–34.

[13]Herbert, T., and Schrauf, G., "Crossflow-Dominated Transition in Flight Tests," AIAA Paper 96-0185, Jan. 1996.

[14]Kaups, K., and Cebeci, T., "Compressible Laminar Boundary Layers with Suction on Swept and Tapered Wings," *Journal of Aircraft*, Vol. 14, No. 7, 1977, pp. 661–667.

[15]Elsholz, E., "Ein inverses LISW-Grenzschicht-Verfahren," MBB Technical Rept. TE2-1681, Nov. 1988.

[16]Schrauf, G., "COAST2—A Compressible Stability Code. User's Guide and Tutorial," DA-Rept. EF11-1973, Oct. 1993.

[17]Stuckert, G., Herbert, T., and Esfahanian, V., "Stability and Transition on Swept Wings," AIAA Paper 93-0078, Jan. 1993.

[18]Schrauf, G., Laburthe, F., and Casalis, G., "Stability Computations on the Long Yawed Cylinder of Poll: Comparison of Stability Codes, Curvature Effects," CERT/ONERA Fiche Technique 2/91, Nov. 1991.

[19]Schrauf, G., "Comparison of Local and Global Amplification Rates Computed with the 'Fixed Frequency/Fixed Wave Length' Strategy," ELFIN II TR 142, Jan. 1995.

[20]Herbert, T., Stuckert, G., and Esfahanian, V., "Effects of Free-Stream Turbulence on Boundary-Layer Transition," AIAA Paper 93-0488, Jan. 1993.

[21]Müller, B., "Experimentelle Untersuchung der Querströmungsinstabilität im linearen und nichtlinearen Bereich des Transitionsgebietes," DLR-Forschungsbericht 90-09, Göttingen, Germany, 1990.

[22]Reibert, M. S., Saric, W. S., Carillo, R. B., "Experiments in Nonlinear Saturation of Stationary Crossflow Vortices in a Swept-Wing Boundary Layer," AIAA Paper 96-0184, Jan. 1996.

[23]Herbert, T., "Secondary Instability of Boundary Layers," *Annual Review Fluid Mechanics*, Vol. 20, 1988, pp. 487–526.